

# Thermalization Mechanisms in Compact Sources

Roland Svensson

*Stockholm Observatory, SE-133 36 Saltsjöbaden, Sweden*

**Abstract.** There is strong observational evidence that a quasi-thermal population of electrons (or pairs) exists in compact X-ray sources. It is, however, unclear what mechanism thermalizes the particles. Here, two processes, Coulomb scattering and synchrotron self-absorption, that may be responsible for the thermalization, are reviewed. The parameter spaces in which respective process dominates are given.

While the Coulomb thermalization mechanism is well-known, this is not the case for the synchrotron self-absorption thermalization. We give the arguments that synchrotron self-absorption must act as a thermalizing mechanism in sufficiently compact sources. The emitting and absorbing electrons then exchange energy efficiently with the self-absorbed synchrotron radiation field and are driven towards a *relativistic* or *mildly relativistic* thermal distribution in a few synchrotron cooling times (the “synchrotron boiler”).

## 1. Introduction

Observations with hard X-ray/ $\gamma$ -ray satellites such as *CGRO* OSSE, *RXTE*, and *BeppoSAX* indicate that the X/ $\gamma$  spectra cut off at a few hundred keV for the majority of active galactic nuclei (see Zdziarski, this volume; Matt, this volume) and for the hard states of galactic black hole candidates (see Zdziarski, this volume; Grove, this volume). It is generally believed that Comptonization by a quasi-thermal population of electrons (or pairs) is responsible for the formation of the X/ $\gamma$  spectra from these sources. In the spectral modeling codes (e.g., Poutanen & Svensson 1996), it is normally assumed that the Comptonizing particles have a Maxwellian distribution. It has been pointed out several times that thermalization by Coulomb scattering may not be fast enough as compared to various cooling mechanisms (such as Compton cooling) and that the particle distribution therefore will differ from a Maxwellian (e.g., Dermer & Liang 1989; Fabian 1994). On the other hand, it has been noticed that another thermalization mechanism, synchrotron self-absorption, may operate in compact plasmas (Ghisellini, Guilbert, & Svensson 1988; Ghisellini & Svensson 1989).

Here, we review the physics of these two thermalization mechanisms, and explore in which contexts each of them may operate.

## 2. Thermalization by Coulomb Scattering

The approximate time scale,  $t_C$ , for thermalization by Coulomb (Møller) scattering between electrons in nonrelativistic plasmas has been known since long (e.g., Spitzer 1956; see Stepney 1983 for relativistic corrections):

$$t_C = 4 \frac{t_T}{\ln \Lambda} \Theta^{3/2} (\pi^{1/2} - 1.2\Theta^{1/4} + 2\Theta^{1/2}), \quad (1)$$

where  $t_T = (n_e \sigma_T c)^{-1}$  is the Thomson time,  $n_e$  is the electron density,  $\ln \Lambda \approx 10 - 20$  is the Coulomb logarithm, and  $\Theta \equiv kT_e/m_e c^2$  is the dimensionless temperature. Only with the advent of X-ray astronomy emerged the understanding that the electrons may reach mildly relativistic temperatures of  $10^9$  K or more, and that electron-positron pairs may be created. In such conditions, electron-positron (Bhabha) scattering also becomes important. Here, the term “Coulomb scattering” will be used for all types of “Coulomb” interactions.

### 2.1. The Relaxation Process

Detailed numerical simulations of the relaxation and thermalization process were performed by Dermer & Liang (1989). As small angle scatterings normally dominate and the fractional energy change per scattering is small, a Fokker-Planck approach is appropriate. Dermer & Liang evaluated the energy exchange and diffusion coefficients assuming the plasma to have a Maxwellian distribution. Using these coefficients in the simulations is equivalent to studying the relaxation of a test particle distribution in a Maxwellian background plasma. Nayakshin & Melia (1998) relaxed the Maxwellian assumption and computed self-consistent Fokker-Planck coefficients using the real particle distributions. A Monte Carlo approach was taken by Pilla & Shaham (1997) who treated the time evolution of both the pair and photon distributions in an infinite system and who besides Coulomb interactions, bremsstrahlung, and Compton scatterings also included pair production and annihilation.

Figure 1 (from Dermer & Liang 1989) shows the relaxation of a test electron distribution in a background thermal electron plasma of temperature 511 keV, or, equivalently,  $\Theta = 1$ . The test electrons had initially a Gaussian distribution centered at 1 MeV and a FWHM of 0.28 MeV. The diffusion process dominates initially and broadens the electron distribution that first relaxes at lower energies and only later the Maxwellian tail forms. Figure 7 in Nayakshin & Melia (1998) shows the similar process but here *all* electrons are initially Gaussian (i.e., there is no Maxwellian background). If the initial distribution is broader than a Maxwellian then the energy exchange coefficient dominates initially and the low energy electrons gain energy while the higher energy electrons loose energy thereby narrowing the distribution towards a Maxwellian (see fig. 6 in Nayakshin & Melia 1998).

### 2.2. Influence of Cooling Processes on the Steady Electron Distribution

With increasing temperature, the Coulomb energy exchange rate decreases. Various cooling processes such as bremsstrahlung, Compton cooling and synchrotron cooling increases with temperature and eventually the thermalization

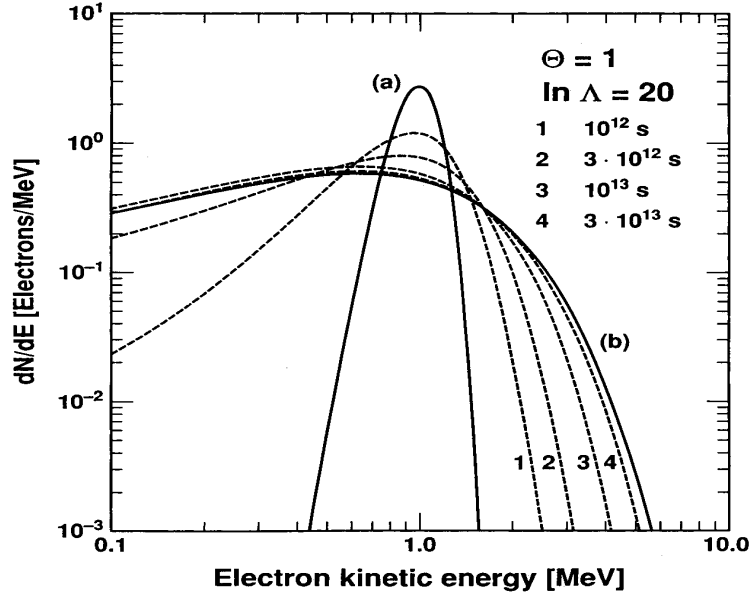


Figure 1. Thermalization through electron-electron scattering of an initially Gaussian electron test distribution (curve a) centered at 1 MeV and a FWHM of 0.28 MeV in a background thermal electron plasma having a Maxwellian distribution of temperature 511 keV, i.e.,  $\Theta = 1$  (curve b). The dashed curves show the relaxing distribution at different times, assuming an electron background density of  $1 \text{ cm}^{-3}$ . The thermalization time scale from eq. (1) is  $2.6 \times 10^{13} \text{ s}$ . From Dermer & Liang (1989).

process will be inhibited by the cooling first noticeable as a truncation of the Maxwellian tail. Stepney (1983) noticed that bremsstrahlung cooling will prevent thermalization for temperatures larger than about  $5 \times 10^{10} \text{ K}$ , and Baring (1987) performed further analysis for additional cooling processes, as did Ghisellini, Haardt, & Fabian (1993).

Including Compton and synchrotron losses in the Fokker-Planck equation allows for the determination of the steady distribution function under the influence of these cooling processes. Results from Dermer & Liang (1989) are shown in Figure 2. It is seen that, for increasing energy densities of radiation and magnetic fields, the high energy tail of the electron distribution becomes increasingly truncated and the effective temperature of the distribution becomes smaller.

What are then the conditions for losses to dominate over Coulomb thermalization (see, e.g., Fabian 1994)? The nonrelativistic cooling time scale can be written as (see Coppi, this volume)

$$t_{\text{cool}} \approx R/[c\ell_B(1 + U_{\text{rad}}/U_B)], \quad (2)$$

where  $R$  is the size of the region,  $\ell_B$  is the magnetic compactness defined in equation (4) below, and  $U_{\text{rad}}$ ,  $U_B$  are the energy densities in radiation and magnetic fields, respectively. Comparing with equation (1), one finds that Coulomb

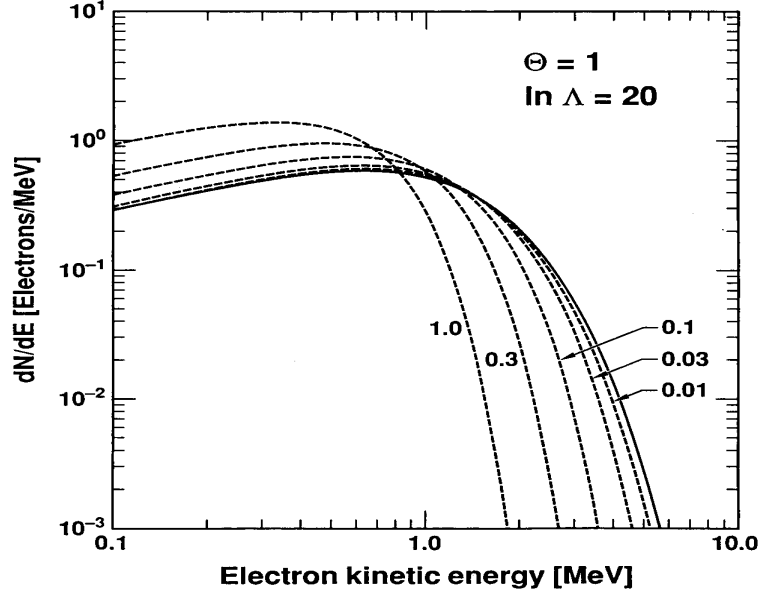


Figure 2. Truncation of a thermal electron distribution with temperature 511 keV due to Compton and synchrotron losses. Solid curve shows a Maxwellian of temperature 511 keV. Dashed curves show the relaxed distributions at different values of the parameter  $(U_{\text{rad}} + U_{\text{B}})/n_e$  in units of MeV. From Dermer & Liang (1989).

scattering cannot maintain a Maxwellian when

$$\ell_{\text{B}}(1 + U_{\text{rad}}/U_{\text{B}}) > \frac{\tau_{\text{T}} \ln \Lambda}{4\Theta^{3/2}}, \quad (3)$$

where  $\tau_{\text{T}} = n_e \sigma_{\text{T}} R$  is the Thomson depth.

### 2.3. Can Coulomb Collisions Thermalize Pair Coronae and Active Pair Regions?

Two different numerical codes (Stern et al. 1995a; Poutanen & Svensson 1996) have been used to study radiative transfer and Comptonization in pure pair coronae in energy and pair balance (see, e.g., Svensson 1997 for a review). For coronae of a given geometry and in energy balance, there exists a unique  $T_e - \tau_{\text{T}}$  relation, where  $T_e$  is the volume-averaged coronal temperature and  $\tau_{\text{T}}$  is a characteristic Thomson scattering optical depth of the coronal region. In Figure 3a, this relation is shown for different geometries. The results for active regions are connected by *dotted* curves. For comparison we also show the slab results from Stern et al. (1995b) using an iterative scattering method code (*dashed curve*).

Solving the pair balance for the obtained combinations of  $(\Theta, \tau_{\text{T}})$  gives a unique dissipation compactness,  $\ell_{\text{diss}}$  (see Ghisellini & Haardt 1994 for a discussion). Here, the local dissipation compactness,  $\ell_{\text{diss}} \equiv (L_{\text{diss}}/h)(\sigma_{\text{T}}/m_e c^3)$ ,

characterizes the dissipation with  $L_{\text{diss}}$  being the power providing uniform heating in a cubic volume of size  $h$  in the case of a slab of height  $h$ , or in the whole volume in the case of an active region of size  $h$ . Figure 3b shows the  $\Theta$  vs.  $\ell_{\text{diss}}$  relations.

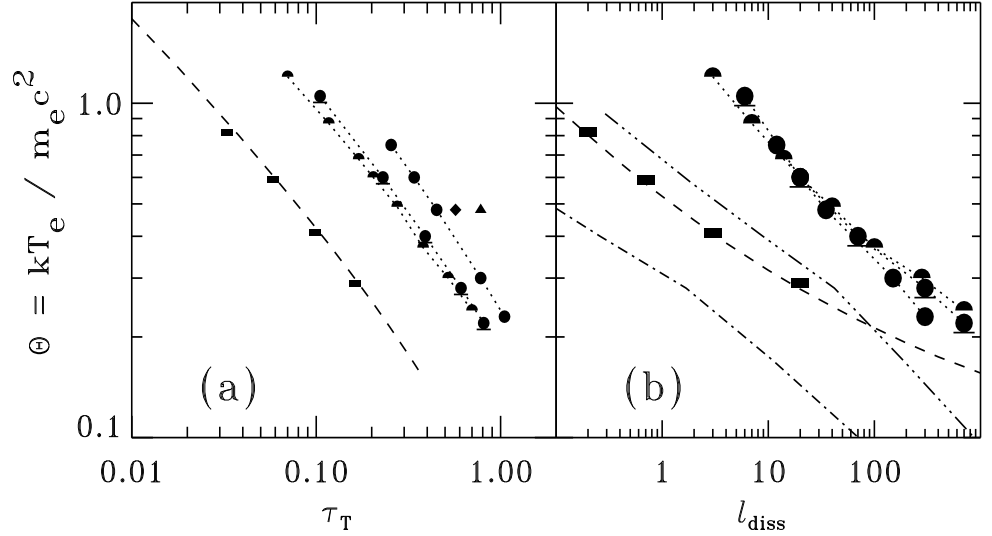


Figure 3. Dimensionless volume-averaged temperature,  $\Theta \equiv kT_e/m_e c^2$ , vs. Thomson scattering optical depth,  $\tau_T$ , in panel (a), and vs. dissipation compactness,  $\ell_{\text{diss}} \equiv (L_{\text{diss}}/h) (\sigma_T/m_e c^3)$  in panel (b), for a steady X-ray emitting plasma region in pair and energy balance on or above a cold disk surface of black body temperature,  $kT_{\text{bb}} = 5$  eV. The plasma Compton scatters reprocessed soft black body photons from the cold disk surface. *Solid rectangles* and *dashed curve* show results from a nonlinear Monte Carlo code (Stern et al. 1995a) and an iterative scattering method code (Poutanen, & Svensson 1996), respectively, for the case of a plane-parallel slab corona. Results using the Monte Carlo code for individual active pair regions are shown for *hemispheres* located on the disk surface; surface spheres also located on the surface (*underlined spheres*); spheres located at a height of  $0.5h$  (*spheres*),  $1h$  (*diamond*), and  $2h$  (*triangle*), where  $h$  is the radius of the sphere. The results for each type of active region are connected by *dotted* curves. The *dash-dotted* and *dash-dot-dot-dotted* curves in panel (b) show the critical compactness as function of  $\Theta$  above which thermalization by Møller and Bhabha scattering is not achieved for the cases of pair slabs and surface spheres, respectively. (Unpublished results by Stern et al.; see also Stern et al. 1995b; Svensson 1997).

The question arises whether the electrons can thermalize or not for the conditions,  $\Theta$ ,  $\tau_T$ , and  $\ell_{\text{diss}}$ , in Figure 3. Energy exchange and thermalization through Møller ( $e^\pm e^\pm$ ) and Bhabha ( $e^+ e^-$ ) scattering compete with various loss mechanisms, with Compton losses being the most important for our conditions. The thermalization is slowest and the Compton losses largest for the higher energy particles in the Maxwellian tail. Instead of using the approximate equation (3), we use the detailed simulations by Dermer & Liang (1989, their fig. 8) to find

the critical compactness above which the deviation of the electron distribution at the Maxwellian mean energy is more than a factor  $e \approx 2.7$ . The *dash-dotted* and *dash-dot-dot-dotted* curves in Figure 3b show this critical compactness for slabs and for surface spheres, respectively. In agreement with Ghisellini, Haardt, & Fabian (1993), we find that Møller and Bhabha scattering cannot compete with Compton losses in our pair slabs and active regions.

The problem then arises of what mechanism can thermalize the apparently thermal electron distribution in compact sources. One such mechanism is cyclo/synchrotron absorption.

### 3. Thermalization by Cyclo/Synchrotron Absorption

#### 3.1. A Brief History of Synchrotron Thermalization

Ever since the classical interpretation by Shklovskii in the 1950s of the radiation from the Crab nebula as being synchrotron radiation, this process has played an important role in our interpretation of the non-thermal radiation from a wide variety of astronomical objects. In general, the electron distribution has been assumed to be a power law or nearly a power law. Much less attention has been paid to what happens to the electron distribution at self-absorbed electron energies.

The theory for synchrotron radiation was developed in the 1950s (see, e.g., reviews by Ginzburg and Syrovatskii 1965, 1969; Pacholczyk 1970). The emission and absorption coefficients for single relativistic electrons as well as for ensembles of relativistic electrons having power law or thermal distributions were calculated in the 1950s and 1960s. For power law distributions, the absorption coefficient increases towards lower photon energies. Below some photon energy,  $\nu_{\text{abs}}$ , the source becomes optically thick to synchrotron self-absorption resulting in an intensity proportional to  $\nu^{5/2}$ , obtained from the ratio of emission and absorption coefficients (Le Roux 1961). A finite  $\nu_{\text{abs}}$ , of course, requires that the source is finite. Below we call this and its consequences "finite source effects".

This early work was, in general, applied to extended sources where the cooling time at self-absorbed particle energies is longer than other relevant time scales (such as the age of the source or the dynamical time scales). It was therefore natural to assume that the self-absorbing electron distribution below the Lorentz factor,  $\gamma_{\text{abs}}$ , of the electron (emitting at the frequency  $\nu_{\text{abs}}$  where the source becomes optically thick) is unaffected by self-absorption and simply maintains the power law distribution of the injected electrons.

In the late 1960s, it became increasingly clear that, in compact sources or on long time scales, the self-absorbed electron distribution  $N(\gamma)$  will evolve under the influence of synchrotron emission and absorption. What are then the possible equilibrium solutions at self-absorbing Lorentz factors towards which  $N(\gamma)$  would relax? In the important papers by Rees (1967) and McCray (1969), it was shown that power law distributions,  $N(\gamma) \propto \gamma^{-s}$  with  $s = 2$  and  $3$ , are equilibrium solutions to the kinetic equations. Rees (1967), however, also found that the solution with  $s = 3$  is unstable and would evolve away from  $s = 3$  if slightly perturbed. McCray (1969) showed this explicitly by numerically calculating the time dependent evolution of initial power law distributions in an infinite source. Rees predicted and McCray confirmed that the high energy electrons

in a flat ( $s < 3$ ) initial power law would tend to evolve into a quasi-Maxwellian distribution. McCray (1969), furthermore, emphasized the importance of finite source effects on the evolution. In particular, for power laws with  $s < 3$ , the self-absorbing electrons would gain energy absorbing slightly more energy than they emit, while the electrons radiating in the optically thin limit lose energy by radiating much more energy than they absorb. All electrons would therefore tend to gather at  $\gamma_{\text{abs}}$  developing a peak there (as was already emphasized by Rees 1967).

It must be emphasized that the relaxation of self-absorbing electrons takes place through the energy exchange with the radiation field, which in its turn is determined by the particle distribution. This is the “synchrotron boiler”, a terminology coined by Ghisellini, Guilbert, & Svensson (1988).

### 3.2. Rise and Fall of yet another Paradigm

In a series of papers in the 1970s, Norman and coworkers further developed the concept *Plasma Turbulent Reactor* (PTR) introduced by Kaplan and Tsytoich (1973). Originally the turbulence feeding the electrons was thought to be plasmons. In practice, however, the PTR is exactly the self-absorbing synchrotron source considered here, as photons are the only plasma modes with sufficiently small damping rate that they can mediate energy transfer from one electron to another (Norman 1977). Norman and ter Haar (1975) and Norman (1977) essentially repeated the analysis of McCray (1969) using quite different notation and definitions but arriving at the same conclusions that  $N(\gamma) \propto \gamma^{-2}$  and  $N(\gamma) \propto \gamma^{-3}$  are the only steady power law equilibrium solutions. It is important that they noted that the  $N(\gamma) \propto \gamma^{-2}$  solution corresponds to a finite electron flux upwards along the energy axis, while  $N(\gamma) \propto \gamma^{-3}$  corresponds to zero electron flux. They argued that  $N(\gamma) \propto \gamma^{-3}$  was the most physical solution as the synchrotron time scales establishing this distribution are shorter than other time scales. Although being aware of possible finite source effects, they considered them not to influence the electron distribution at Lorentz factors  $\ll \gamma_{\text{abs}}$ .

The self-absorbed solution,  $N(\gamma) \propto \gamma^{-3}$ , was considered sufficiently important in explaining power law spectra from a variety of sources that Norman and ter Haar (1975) called the PTR a *new astrophysical paradigm*. Norman and coworkers, however, do not seem to have considered the stability of the  $N(\gamma) \propto \gamma^{-3}$  solution.

The work of Rees (1967) and McCray (1969) indicates that a Maxwellian distribution may be the only *stable* equilibrium solution. This was, however, not rigorously established causing Ghisellini, Guilbert & Svensson (1988, GGS88) to numerically determine the steady solutions of the kinetic equations including physical boundary conditions (i.e., correct Fokker-Planck coefficients at subrelativistic energies, and the accounting for finite source effects at large energies). As  $\gamma_{\text{abs}}$  typically is of the order 10-100 in compact radio sources and the development of the self-absorbed distribution takes place at mildly relativistic energies, they used expressions and equations valid at any energy. Furthermore, in order to obtain steady solutions the particle injection had to be balanced by a sink term (escape or reacceleration). Injecting a power law proportional to  $\gamma^{-3}$  (i.e., with the equilibrium slope) GGS88 found that the steady solution was a *Maxwellian* with a temperature corresponding to the mean energy of the in-

jected electrons. Similarly, an injected power law proportional to  $\gamma^2$  (essentially corresponding to monoenergetic injection at some large Lorentz factor  $\gg \gamma_{\text{abs}}$ ) led to the establishment of a Maxwellian just below  $\gamma_{\text{abs}}$ . The injected electrons cool until reaching  $\gamma_{\text{abs}}$  where they thermalize exchanging energy with the self-absorbed radiation field. Additional studies were made by de Kool, Begelman, & Sikora (1989) and Coppi (1990). With these works it appears that the PTR paradigm of Norman and ter Haar (1975) has been shown to be invalid.

### 3.3. Relaxation by Cyclo/Synchrotron Absorption

The works so far that explicitly have *demonstrated* the formation of a Maxwellian through synchrotron self-absorption are the numerical simulations of GGS88, Coppi (1990), and Ghisellini, Haardt, & Svensson (1998). Here, we review some of the results in the last paper. In the numerical simulations, a kinetic equation for the electron distribution is solved. The kinetic equation, which also in this case takes the form of a Fokker-Planck equation (see derivation in McCray 1969), includes Compton and synchrotron cooling, synchrotron absorption (heating), electron injection, and electron escape. Even though various source geometries are discussed, the radiation field is assumed to be given by the steady slab solution, which is correct to the order of unity.

The simulations consider a region of size  $R$  with a magnetic field of strength  $B$ , into which some distribution of electrons are injected with a power  $L$ . In a steady state, this power emerges either as radiation or as the power of escaping electrons. The electrons are assumed to escape at the speed  $v_{\text{esc}} = c\beta_{\text{esc}} = R/t_{\text{esc}}$  where  $t_{\text{esc}}$  is the escape time. Convenient parameters describing compact sources are the injection compactness,  $\ell_{\text{inj}}$ , and the magnetic compactness,  $\ell_{\text{B}}$ , defined as

$$\ell_{\text{inj}} = \frac{L}{R} \frac{\sigma_{\text{T}}}{m_e c^3}; \quad \ell_{\text{B}} = \frac{\sigma_{\text{T}}}{m_e c^2} R U_{\text{B}}, \quad (4)$$

where  $\sigma_{\text{T}}$  is the Thomson cross section and  $U_{\text{B}} = B^2/8\pi$  is the magnetic field energy density. Note that  $U_{\text{rad}}/U_{\text{B}} \approx (9/16\pi)(\ell_{\text{inj}}/\ell_{\text{B}})(1 + \tau_{\text{T}})$ , where the numerical factor is dependent on the source geometry. The problem we consider has the following parameters:  $\ell_{\text{inj}}$ ,  $\ell_{\text{B}}$ ,  $\beta_{\text{esc}}$ , and either  $R$  or  $B$ . Further parameters are those describing the shape of the injected electron distribution.

For steady state electrons emitting and absorbing synchrotron photons, the cooling (emission) and absorption/diffusion time scales are balanced and thus equal. The synchrotron cooling time scale can thus be taken to be the thermalization time scale. From Equation (2), it is then clear that self-absorbing electrons will thermalize before they escape when  $\ell_{\text{B}} \gtrsim 1$ . The simulations shown below have  $\ell_{\text{B}} = 10$  and 30.

Figure 4 shows the relaxation due to cyclo/synchrotron absorption of an electron distribution towards the equilibrium Maxwellian distribution. The injected electrons have a Gaussian energy distribution peaking at  $\gamma = 10$ . Each curve is labeled by the time in units of  $R/c$ . The shape of the equilibrium distribution is reached in about  $\sim 0.1R/c$ , about equal to the cyclo/synchrotron cooling time. With the assumed input parameters, the synchrotron terms (emission, absorption and energy diffusion) in the kinetic equation are dominant over Compton losses. Gains and losses in this case almost perfectly balance. As a result the equilibrium electron distribution is a Maxwellian. Figure 4 also shows



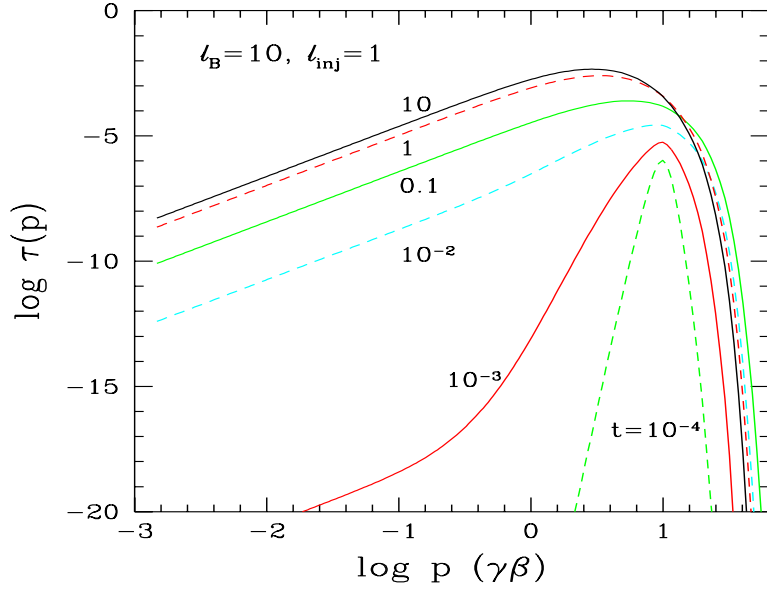


Figure 4. Electron distribution,  $\tau(p) \equiv \sigma_T RN(p)$ , evolving due to cyclo/synchrotron emission/absorption/diffusion. Curves are labeled by times in units of  $R/c$ . Parameters are  $\ell_{\text{inj}} = 1$ ,  $\ell_B = 10$ ,  $R = 10^{13}$  cm (or  $B \simeq 5.5 \times 10^3$  G), and  $\beta_{\text{esc}} = 1$ . The injected distribution is a Gaussian centered at  $\gamma = 10$ . From Ghisellini, Haardt, & Svensson (1998).

that the high energy part of the Maxwellian distribution is formed earlier than the low energy part, due to the higher efficiency of exchanging photons of the high energy electrons. A slower evolution takes place after  $0.1(R/c)$ , as the balance between electron injection and electron escape is achieved on a time scale of a few  $t_{\text{esc}}$ . Only then have both the shape and the amplitude of the electron distribution reached their equilibrium values.

### 3.4. Influence of Cooling Processes on the Steady Electron Distribution

The equilibrium distributions for different values of the injected compactness are shown in Figure 5. The magnetic compactness is set to  $\ell_B = 30$ , corresponding to  $B = 10^4$  G for  $R = 10^{13}$  cm (from Eq. 4). In all cases, the injected distribution is a peaked function with an exponential high energy cut-off. The mean injected Lorentz factor is  $\langle \gamma \rangle \simeq 5$  and essentially all electrons are below  $\gamma_{\text{abs}}$ . It is apparent from Figure 5 that the electron distribution is a quasi-Maxwellian at all energies as long as  $\ell_{\text{inj}} \ll \ell_B$ . This is a consequence of an almost perfect balance between synchrotron gains (absorption) and losses, while Compton losses are only a small perturbation. As  $\ell_{\text{inj}}$  increases towards  $\ell_B$ , Compton losses become increasingly important, competing with the synchrotron processes. At high energies, losses overcome gains, and the electrons diffuse downwards in energy, until subrelativistic energies are reached. In this energy regime, the increased

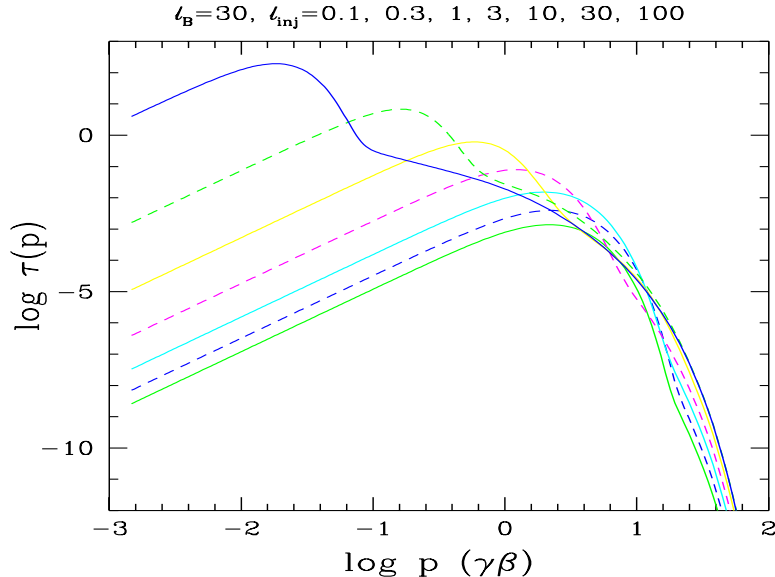


Figure 5. Steady equilibrium electron distributions due to cyclo/synchrotron emission/absorption/diffusion and Compton cooling for different injected compactnesses (decreasing from top to bottom). Further parameters are  $\ell_B = 30$ ,  $R = 10^{13}$  cm,  $\beta_{\text{esc}} = 1$ . The corresponding magnetic field is  $B = 10^4$  G. The mean injected Lorenz factor is about 5. Increasing  $\ell_{\text{inj}}$  implies increased Compton cooling resulting in a shift of the quasi-Maxwellian towards lower temperatures. From Ghisellini, Haardt, & Svensson (1998).

efficiency of synchrotron gains (relative to losses) halts the systematic downward diffusion in energy, and a Maxwellian can form (see Ghisellini & Svensson 1989). The temperature of this part of  $N(\gamma)$  can be obtained by fitting a Maxwellian to the the low energy part of the distribution, up to energies just above the peak of the electron distribution.

The resulting temperatures are plotted in Figure 6 as a function of  $\ell_{\text{inj}}$ . For  $\ell_{\text{inj}} \lesssim 1$ , the temperature is approximately constant, while it decreases for  $\ell_{\text{inj}} \gtrsim 1$ . From Equation (3) (with  $U_{\text{rad}}/U_B$  set to zero), we see that thermalization by synchrotron self-absorption dominates when  $\ell_B > \tau_T \ln \Lambda / 4\Theta^{3/2}$  (assuming  $\Theta \lesssim 1$ ). The Coulomb process thus dominates for small temperatures and large  $\tau_T$  (i.e., large electron densities). We need to know  $\tau_T$  for our simulations. The balance between electron injection and escape in our model gives a Thomson optical depth of  $\tau_T = (3/4\pi)(\ell_{\text{inj}}/\beta_{\text{esc}} < \gamma >)$ . For the simulations in Figure 5, the optical depth increases from  $\tau_T = 5 \times 10^{-3}$  for  $\ell_{\text{inj}} = 0.1$  to  $\tau_T = 5$  for  $\ell_{\text{inj}} = 100$ . Using the expression for  $\tau_T$ , we find that thermalization by synchrotron self-absorption then dominates over Coulomb scattering for temperatures  $\Theta > 0.11(\ln \Lambda / < \gamma >)^{2/3}(\ell_{\text{inj}}/\ell_B)^{2/3}$ . For the parameters of the simulations in Figures 5 and 6 and  $\ln \Lambda = 20$ , the condition becomes  $\Theta > 0.03(\ell_{\text{inj}})^{2/3}$ , which is plotted as the solid line in Figure 3. One sees that

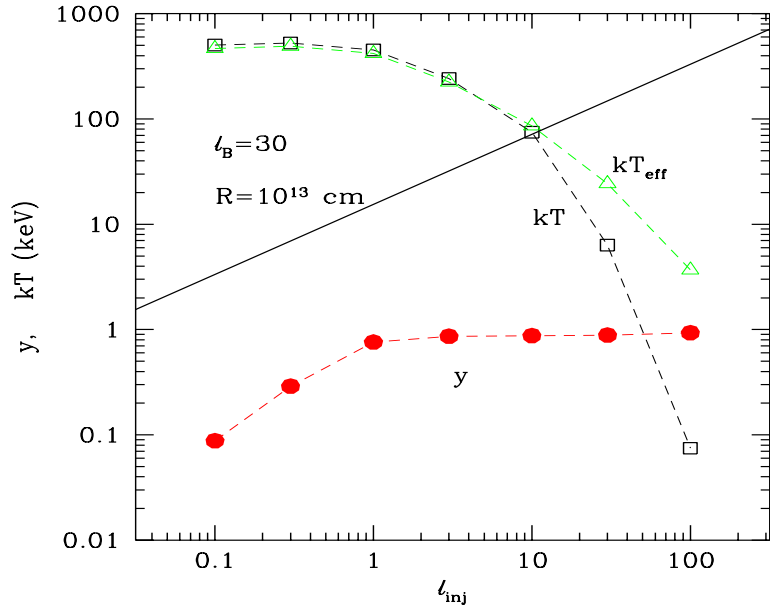


Figure 6. Temperatures of the quasi-Maxwellian part of steady equilibrium electron distributions shown in Fig. 5. Above the solid line, synchrotron self-absorption dominates over Coulomb exchange as the thermalization mechanism. The solid dots show the Comptonization  $y$ -parameter. From Ghisellini, Haardt, & Svensson (1998).

that synchrotron self-absorption dominates the thermalization for all cases with  $\ell_{\text{inj}}$  smaller than about 10. For the cases  $\ell_{\text{inj}} = 30$  and 100, one cannot neglect Coulomb thermalization.

### 3.5. Spectra from Steady Electron Distributions

In Figure 7, the radiation spectra corresponding to four of the equilibrium electron distributions in Figure 5 are shown. Each spectrum consists of several continuum components:

- a self-absorbed synchrotron spectrum (S);
- a Comptonized synchrotron spectrum (SSC);
- a reprocessed thermal soft component (bump);
- a component from Comptonization of thermal bump photons (IC);
- a Compton reflection component.

Details of the spectral calculations are given in Ghisellini, Haardt, & Svensson (1998). Some features in Figure 7 may be noticed. For  $\ell_{\text{inj}} < 1$ , the Compton  $y$ -parameter is less than unity (see Fig. 6) making the Compton losses relatively unimportant relative the self-absorbed synchrotron radiation. The large value of

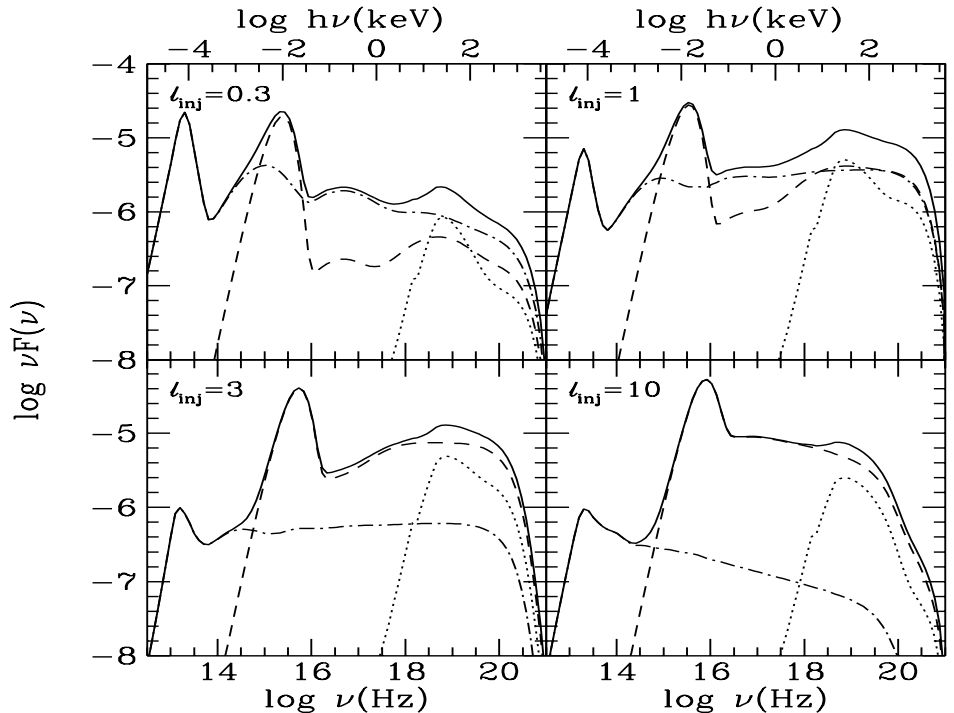


Figure 7. Radiation spectra calculated using four of the electron distributions shown in Fig. 5. The different spectral components are the reprocessed thermal bump and IC components (dashed curves), the synchrotron and SSC components (dash-dotted curves), and the Compton reflection component (dotted curves). The total spectra are shown by the solid curves. Note that the chosen parameters ( $R = 10^{13}$  cm, and the corresponding magnetic field  $B = 10^4$  G) correspond to conditions expected near black holes in active galactic nuclei. From Ghisellini, Haardt, & Svensson (1998).

$\Theta$  makes the Comptonized spectra bumpy. The 2–10 keV band is dominated by the SSC component, rather than by the IC. The thermal bump and the X-ray flux are thus not directly related. This is contrary to the common interpretation of the X-ray emission in Seyfert galaxies as being due to Comptonization of thermal bump photons.

For  $\ell_{\text{inj}} > 1$ , the Compton cooling dominates and limits the  $y$ -parameter to unity. The smooth IC power law dominates over the S and SSC components. For  $\ell_{\text{inj}} \lesssim 3$ , the high energy spectral cut-off can be described by an exponential, since the electron distribution is a quasi-Maxwellian in the entire energy range. For  $\ell_{\text{inj}} \gtrsim 3$ , the electron distribution is more complex (see Fig. 5), resulting in a more complex spectral cut-off.

The choice of  $R = 10^{13}$  cm (or  $B = 10^4$  G) in Figure 7 corresponds to the case of active galactic nuclei (AGN). Ghisellini, Haardt, & Svensson (1998) also study the case of galactic black holes choosing  $R = 10^7$  cm (or  $B = 10^7$  G) for

the same set of  $\ell_B$  and  $\ell_{inj}$ . The large magnetic field and small size move the S and bump peaks to larger frequencies. The main difference is that now the synchrotron component is not completely self-absorbed leading to an optically thin synchrotron component from the highest energy electrons. More soft synchrotron photons enhances the SSC component relative the IC component as compared to the AGN case.

#### 4. Final Remarks

First, we note that  $\ell_B > 1$  is needed for synchrotron self-absorption to operate efficiently (from eq. 2). A Maxwellian is then formed with the same mean energy as the injected electrons, assuming that self-absorption operates at essentially all electron energies of interest. If, furthermore, Compton cooling is important, i.e., if  $\ell_{inj} > \ell_B$ , then the Maxwellian is modified and is shifted to lower energies (temperature).

Second, we note that the criterion for Coulomb vs synchrotron thermalization in the case when all electrons are self-absorbing (i.e. radiating optically thick synchrotron radiation) is more complex (eq. 3). Essentially, the same criterion is valid for comparing Coulomb thermalization in the case when the major part of the electrons radiate optically thin synchrotron radiation (or Compton radiation) truncating the Maxwellian. Which of the two cases that is valid depends on whether the energy,  $(\gamma_{abs} - 1)m_e c^2$ , of the electrons radiating at the photon energy where the absorption optical depth is unity is much larger or much smaller than  $kT_e$ .

There should also be a region in parameter space where both Coulomb and synchrotron thermalization operates simultaneously (assuming that most electrons radiate optically thick radiation). Here, Coulomb thermalization should dominate at lower electron energies and synchrotron thermalization at larger energies. However, nobody seems so far to have solved the Fokker-Planck equations to study the thermalization process including both Coulomb scattering and synchrotron self-absorption.

Ultimately, the thermalization process should be put in a realistic context. Mahadevan & Quataert (1997) studied the importance of thermalization in advection-dominated flows onto black holes under the conditions considered in such flows (e.g., close to free-fall, equipartition magnetic fields). Comparing the thermalization time scales with the accretion time scale (equivalent to  $t_{esc}$  in our discussion), they found that thermalization did not occur at large radii and small accretion rates. However, at sufficiently large accretion rate, synchrotron thermalization becomes important, and at even larger rates (and thus larger densities) Coulomb thermalization starts operating.

Another scenario for generating the X-ray radiation from compact sources is that of a corona or magnetic flares atop an accretion disks. The typical condition for the flare regions is that the magnetic energy density should dominate the radiation energy density, i.e., that  $\ell_B \gtrsim \ell_{inj} > 1$ , which should ensure that cyclo/synchrotron self-absorption acts as a very efficient thermalizing mechanism in such regions.

**Acknowledgments.** I appreciate a more than decade-long collaboration with G. Ghisellini on the issues discussed in this review. I thank J. Poutanen and A. Beloborodov for valuable comments. This work is supported by the Swedish Natural Science Research Council and the Swedish National Space Board.

## References

- Baring, M. 1987, MNRAS, 228, 695  
Coppi, P. S. 1992, MNRAS, 258, 657  
de Kool, M., Begelman, M. C., & Sikora, M. 1989, ApJ, 337, 66  
Dermer, C. D., & Liang, E. P. 1989, ApJ, 339, 512  
Fabian, A. C. 1994, ApJS, 92, 555  
Ghisellini, G., Guilbert, P. W., & Svensson R. 1988, ApJ, 334, L5 (GGS88)  
Ghisellini, G., & Haardt, F. 1993, ApJ, 429, L53  
Ghisellini, G., Haardt, F., & Fabian, A. C. 1993, MNRAS, 263, L9  
Ghisellini, G., Haardt, F., & Svensson, R. 1998, MNRAS, 297, 348  
Ghisellini, G., & Svensson, R. 1989, in Physical processes in hot cosmic plasmas, eds. Brinkmann, W., Fabian, A. C. & Giovannelli, F., NATO ASI Series, Kluwer Academic Publishers, 395  
Ginzburg, V. L., & Syrovatskii, S. I. 1965, ARA&A, 3, 297  
Ginzburg, V. L., & Syrovatskii, S. I. 1969, ARA&A, 7, 375  
Kaplan, S. A., & Tsytovich, V. N. 1973, Plasma Astrophysics, Elmsford, N.Y.: Pergamon  
Le Roux, E. 1961, Annals Astrophys., 24, 71  
Mahadevan, R., & Quataert, E. 1997, ApJ, 490, 605  
McCray, R. 1969, ApJ, 156, 329  
Nayakshin, S., & Melia, F. 1998, ApJS, 114, 269  
Norman, C. A. 1974, Fysisk Tidskrift (Møller Festschrift), 72, 84  
Norman, C. A. 1977, Annals of Physics, 106, 26  
Norman, C. A., & ter Haar, D. 1975, Physics Reports, 17, 309  
Pacholczyk, A. G. 1970, Radio Astrophysics, San Francisco: Freeman  
Pilla, R. P., & Shaham, J. 1997, ApJ, 486, 903  
Poutanen, J., & Svensson, R. 1996, ApJ, 470, 249  
Rees, M. J. 1967, MNRAS, 136, 279  
Spitzer, L. 1956, Physics of Fully Ionized Gases, New York: Wiley  
Stepney, S. 1983, MNRAS, 202, 467  
Stern, B. E., Begelman, M. C., Sikora, M., & Svensson, R. 1995a, MNRAS, 272, 291  
Stern, B. E., Poutanen, J., Svensson, R., Sikora, M., & Begelman, M. C. 1995b, ApJ, 449, L13  
Svensson, R. 1997, in Relativistic Astrophysics: A Conference in Honour of Professor I. D. Novikov's 60th Birthday, eds. B. J. T. Jones and D. Markovic, Cambridge: Cambridge University Press, 235